Coronado, Irene; Pitínová, Martina; Karinen, Reetta; Reinikainen, Matti; Puurunen, Riikka L.; Lehtonen, Juha

Aqueous-phase reforming of Fischer-Tropsch alcohols over nickel-based catalysts to produce hydrogen

Published in:
Applied Catalysis A: General

DOI:
10.1016/j.apcata.2018.09.013

Published: 25/10/2018

Document Version
Publisher's PDF, also known as Version of record

Applied Catalysis A, General 567 (2018) 112–121

Contents lists available at ScienceDirect

Applied Catalysis A, General

journal homepage: www.elsevier.com/locate/apcata

Aqueous-phase reforming of Fischer-Tropsch alcohols over nickel-based catalysts to produce hydrogen: Product distribution and reaction pathways

Irene Coronado[a,*], Martina Pitínová[b,1], Reetta Karinen[b], Matti Reinikainen[a], Riikka L. Puurunen[b], Juha Lehtonen[a]

[a] VTT Technical Research Centre of Finland Ltd., Espoo, FI-02044 VTT, Finland
[b] Department of Chemical and Metallurgical Engineering, School of Chemical Engineering, Aalto University, Espoo, 02150, Finland

ARTICLE INFO

Keywords:
Aqueous-phase reforming
Alcohols
Hydrogen
Nickel-based catalysts
Fischer-Tropsch water fraction

ABSTRACT

Catalytic aqueous-phase reforming (APR) can be applied to process the organic compounds in the water fractions derived from the Fischer-Tropsch (FT) synthesis. This work aimed at finding an active nickel-based catalyst to convert organic compounds typically found in FT-derived waters, such as alcohols, into hydrogen. In addition, this work aimed at proposing potential reaction pathways that explain the product distribution resulting from the APR of C_1–C_3 alcohols. Solutions with 5% mass fraction of either methanol, ethanol, propan-1-ol or propan-2-ol in water were processed in APR at 230 °C and 3.2 MPa over different nickel-based catalysts in a continuous packed-bed reactor. Methanol was successfully reformed into hydrogen and carbon monoxide with conversions up to 60%. The conversion of C_2–C_3 alcohols achieved values in the range of 12% to 55%. The results obtained in the APR of C_2–C_3 alcohols suggest that in addition to reforming to hydrogen and carbon monoxide, the alcohols underwent dehydrogenation and decarbonylation. The most stable catalyst, nickel-copper supported on ceria-zirconia, reached feedstock conversions between 20% and 60% and high hydrogen selectivity. Monometallic nickel supported on ceria-zirconia catalysts reached higher H_2 yields; however, the yield of side products, such as alkanes, was also higher over the monometallic catalysts. Accordingly, ceria-zirconia nickel-based supported catalysts constitute suitable candidates to process the alcohols in the water fractions derived from the FT synthesis.

1. Introduction

The water fraction derived from the Fischer-Tropsch (FT) process contains organic, water-soluble compounds that are challenging for conventional wastewater treatment processes [1]. These compounds consist of oxygenated hydrocarbons such as alcohols that can be converted into valuable products including hydrogen by aqueous-phase reforming (APR) [2,3]. The conversion of the alcohols in the FT water fraction into hydrogen may enhance the economic efficiency of renewable fuel production through FT-synthesis and reduce the organic content in the water fraction directed to wastewater treatment.

Aqueous-phase reforming takes place at low temperatures, 200 °C to 250 °C, and above the bubble point pressure of the feedstock [4], avoiding an energy demanding evaporation step. APR constitutes a suitable candidate to process wastewater with diluted organic compounds because it is energetically efficient compared to steam and autothermal reforming [5]. The energy efficiency becomes significant because evaporation of the highly diluted organic solution is avoided in APR. Consequently, a number of research groups have studied the APR of oxygenated hydrocarbons [6–8]. The mass fraction of oxygenated hydrocarbons in the water stream from the FT process is typically below 10%. A mixture of short-chain alcohols (C_1-C_3) is the largest group of organic constituents in the FT water fraction [9,10]. Although polyols such as ethylene glycol and glycerol have been the main model compounds applied in APR, monohydric alcohols have also been considered [3]. Methanol [11–14] and ethanol [15,16] were model compounds in APR for hydrogen production over platinum-based catalyst. Iridium supported on different metal oxides was also utilized as catalyst in the APR of methanol [17], and iridium, rhodium and rhenium supported on TiO_2 in the APR of ethanol [18,19]. The APR of ethanol has been additionally conducted over nickel-based catalyst supported on hydrotalcite-like compounds [20], alumina [21], and ceria [22]. The APR of C_3 alcohols has been investigated over Pt-based catalysts supported on alumina [23,24] and on polymer-derived carbon [25]. Moreover, real

* Corresponding author.
E-mail address: irene.coronado@vtt.fi (I. Coronado).
[1] Present address: J. Heyrovsky Institute of Physical Chemistry of the Czech Academy of Sciences, Prague 8, 182 23, Czech Republic.

https://doi.org/10.1016/j.apcata.2018.09.013
Received 12 July 2018; Received in revised form 13 September 2018; Accepted 15 September 2018
Available online 19 September 2018
0926-860X/

FT derived water fractions have been processed over Ru supported on active carbon and on metal oxides to produce alkanes via hydrodeoxygenation [26,27].

In a previous work on the APR of methanol, doping of nickel on alumina with copper or cerium enhanced the hydrogen production compared to the monometallic catalyst [28]. Furthermore, nickel on ceria-zirconia catalysts exhibited high performance in terms of methanol conversion and hydrogen production [29]. Several authors have similarly described the positive effect of cerium on the catalyst activity in APR. This effect has been attributed to oxygen vacancies that may promote reforming to hydrogen and carbon monoxide, and the conversion of carbon monoxide through the water-gas shift (WGS) reaction. The addition of cerium may also enhance the stability of the catalyst [22,30–36]. Furthermore, copper has been applied as a catalyst dopant to improve the hydrogen selectivity in APR by limiting the formation of side products such as alkanes [37–39].

This work focuses on comparing the APR of methanol, ethanol, propan-1-ol and propan-2-ol. Water solutions of these alcohols were selected as model feedstock because they are representative of the FT-derived water fraction. Self-prepared nickel catalyst on ceria-zirconia supports with different ceria contents, and nickel doped with cerium on γ-alumina were selected due to their high activity and hydrogen selectivity, reported in previous studies [28,29]. Furthermore, nickel doped with copper or cerium supported on ceria-zirconia were considered as potential catalysts to improve the hydrogen production in APR. The results obtained from the APR of C_1-C_3 alcohols elucidate the effect of alcohol chain-length, the influence of the location of the hydroxyl group in alcohols and the type of catalyst applied on the reaction pathway and the product distribution.

2. Experimental

2.1. Materials

Ceria-zirconia supports with mass percentage of ceria in zirconia equal to 17% or 25% were supplied by MEL Chemicals in powder form. Engelhard supplied the γ-Al_2O_3 support. The metal precursors used in impregnation were nickel ($Ni(NO_3)_2{\cdot}6H_2O$, ≥97.0%), copper ($Cu(NO_3)_2{\cdot}3H_2O$, 99–104%) and cerium ($Ce(NO_3)_3{\cdot}6H_2O$, ≥99.0%) nitrates. These chemicals were supplied by Sigma-Aldrich. The feedstock were aqueous solutions with 5% mass fraction of either methanol (MeOH), ethanol (EtOH), propan-1-ol (1-PrOH) or propan-2-ol (2-PrOH). The chemicals were supplied by VWR Chemicals (assay on anhydrous substance is 100%), Altia Industrial (Etax Aa, assay of 99.5%), VWR Chemicals (assay of 100%) and Fluka (assay of > 99.9%) respectively.

2.2. Preparation and characterization of catalysts

The catalysts listed in Table 1 were prepared through incipient wetness impregnation, similarly as in [29]. The ceria-zirconia supports were calcined at 450 °C for 10 h in flowing synthetic air, pelletized, crushed and sieved to 200–300 μm prior to metal impregnations. The bimetallic catalysts supported on 25% ceria-zirconia were prepared through co-impregnation of nickel and copper or cerium precursors in water solutions. After impregnating the metal precursors on 17% and 25% ceria-zirconia supports, the impregnated materials were kept for 24 h at room temperature, followed by drying at 110 °C and calcination in flowing air at 500 °C for 4 h. The bimetallic catalyst supported on γ-Al_2O_3 was prepared through sequential impregnation of first cerium precursor followed by nickel precursor. The catalyst was dried at 80 °C under vacuum and calcined at 500 °C for 2 h in flowing air after impregnation. Prior to the APR experiments, the catalysts were reduced in situ at 450 °C and 2.5 MPa for 2 h with a H_2:N_2 = 1 gas flow of 10 $dm^3\ h^{-1}$. The values of target mass percentage included in Table 1 were calculated as the mass of metal in zero oxidation state per total mass of catalyst.

Table 1
List of catalysts and target contents of impregnated metals.

Catalyst	ID	Ni target (mass fraction)	Cu or Ce impregnated target (mass fraction)
Ni/17 % CeO_2-ZrO_2	Ni/17CeZr	10%	n.a.
Ni/25 % CeO_2-ZrO_2	Ni/25CeZr	10%	n.a.
Ni-Cu/25 % CeO_2-ZrO_2	NiCu/25CeZr	10%	5.0%
Ni-Ce/25 % CeO_2-ZrO_2	NiCe/25CeZr	10%	5.0%
Ni-Ce/γ-Al_2O_3	NiCe/Al	13%	1.3%

n.a.: not applicable.

The equipment and methods utilized for the characterization of catalysts were detailed in [29] and briefly described here. The supports, after calcination in the case of mixed-oxide materials, calcined catalysts and spent catalysts were characterized using atomic absorption spectroscopy (AAS) and inductively coupled plasma - optical emission spectroscopy (ICP-OES) to analyse metal loadings. For the AAS, 200 mg of catalyst was dissolved in aqua regia at 120 °C and subsequently diluted with Milli-Q water. Ni and Cu loadings were determined with a Varian AA240 AAS equipment applying air-acetylene flame, and Ce loading with a Perkin Elmer 7100 ICP-OES. Nitrogen physisorption was applied to determine BET surface areas and BJH method to determine pore volumes and pore sizes distribution. Nitrogen physisorption was conducted in an Thermo Fisher Ultra Surfer after degassing the calcined catalyst samples at 200 °C for 3 h in vacuum, and the samples of spent catalysts at 120 °C for 5 h. X-ray diffraction (XRD) was conducted to identify crystalline phases and to determine the crystallite sizes of nickel species. A PANalytical X-pert PRO MPD Alpha-1 diffractometer with Cu Kα1 radiation (45 kV and 40 mA) was utilized to obtain the XRD data. The scanning was continuous and ranged from 10° to 90° (2Θ) with step size of 0.0131°. Based on peak broadening, Scherrer equation [40] was applied to estimate the particle size of nickel species. The X-Ray wavelength of Cu K-alpha was assumed to be 0.154 nm, and a crystallite shape-factor of 0.94 was applied, considering sphere-like catalyst particles. Attempts to identify nickel species and determine their particle size with a scanning transmission electron microscope (STEM) were made with no success. In the results form STEM, Ni species were not detected, most likely because the atomic weight of nickel is considerably lower than the atomic weight of the metals in the support, cerium and zirconium [29].

2.3. Aqueous-phase reforming of alcohols

Aqueous solutions prepared with Milli-Q water and 5% mass fraction of either MeOH, EtOH, 1-PrOH or 2-PrOH were processed in APR over the catalysts listed in Table 1. The experiments were conducted over 1.5 g of catalyst in a continuous fixed-bed reactor described in detail elsewhere [29]. The gaseous products were analysed with an online Agilent 490 Micro GC Biogas Analyzer with two thermal conductivity detectors (TCD), and the liquid products were analysed offline with an Agilent GC 6890 series with a flame ionization detector (FID) according to the detailed methods described in [29]. The operating conditions were set to be 230 °C, 3.2 MPa of inlet pressure, and 2.0 $cm^3\ min^{-1}$ of aqueous solution flow.

Ideally, the reforming of MeOH, EtOH, 1-PrOH or 2-PrOH results in the formation of H_2 and CO (Eqs. 1–4). At low temperatures, the WGS reaction (Eq. 5) is favoured to convert CO with H_2O into CO_2 and H_2. The Gibbs free energy changes presented in this work were calculated at 503 K with HSC Chemistry 8, software from Outotec. In addition to the APR operating conditions, potentially spontaneous reactions (Eqs. 2–4) due to slightly positive Gibbs free energy changes [41], and the type of

catalyst and feedstock may facilitate different reaction pathways and the formation of side products, for instance through hydrogenation of carbon oxides (Eqs. 6 and 7). Accordingly, full reforming denotes in this work the reaction where the alcohol in the feedstock is converted into H_2 and CO; and aqueous-phase reforming is considered as the process where different reactions, in addition to full reforming, such as WGS, and side reactions including methanation may take place.

Methanol full reforming:

$$CH_3OH(l) \xleftrightarrow{H_2O} CO\,(g) + 2H_2\,(g) \quad \Delta G_{503} = -24.8\,kJ \tag{1}$$

Ethanol full reforming:

$$C_2H_5OH\,(l) + H_2O(l) \leftrightarrow 2CO\,(g) + 4H_2\,(g) \quad \Delta G_{503} = +8.5\,kJ \tag{2}$$

Propan-1-ol full reforming:

$$C_3H_7\,OH + 2H_2O\,(l) \leftrightarrow 3CO\,(g) + 6H_2\,(g) \quad \Delta G_{503} = +19.9\,kJ \tag{3}$$

Propan-2-ol full reforming:

$$C_3H_7\,OH + 2H_2O(l) \leftrightarrow 3CO\,(g) + 6H_2\,(g) \quad \Delta G_{503} = +47.1\,kJ \tag{4}$$

WGS reaction:

$$CO\,(g) + H_2O\,(l) \leftrightarrow CO_2(g) + H_2\,(g) \quad \Delta G_{503} = -33.6\,kJ \tag{5}$$

CO_x hydrogenation

$$CO\,(g) + 3H_2\,(g) \leftrightarrow CH_4(g) + H_2O\,(l) \quad \Delta G_{503} = -82.1\,kJ \tag{6}$$

$$CO_2\,(g) + 4H_2\,(g) \leftrightarrow CH_4(g) + 2H_2O\,(l) \quad \Delta G_{503} = -67.1\,kJ \tag{7}$$

The results presented in this work are based on product analyses taken at approximately 6 h on stream, when the amount of gases in the outlet stream had stabilized to nearly constant concentrations after a gradual increase. The parameters used to evaluate the experimental results are mass balance (MB, Eq. 8), conversion (X, Eq. 9), selectivity to liquid products (S^k, Eq. 10), hydrogen production rate (H_2 PR, Eq. 11), hydrogen efficiency (H_2 Eff, Eq. 12), hydrogen molar fraction among gaseous products (x^{H2}, Eq. 13), yield of gaseous compounds (Y^i, Eq. 14) and yield of liquid compounds (Y^k, Eq. 15). Eq. 12 includes a H_2/CO_2 stoichiometric reforming ratio (RR) that has been traditionally used to evaluate the efficiency of H_2 production [42]. This factor considers the stoichiometric production of H_2 through full reforming (Eqs. 1–4) and WGS reactions (Eq. 5). Therefore, RR equals to 3 for MeOH, 6 for EtOH, and 9 for 1-PrOH and 2-PrOH. The H_2 molar fraction in Eq. 13 evaluates the fraction of H_2 produced among gases, and liquid products are disregarded in this formula. In addition, when referred to H_2, Eq.14 considers the amount of H_2 in the outlet stream per amount of alcohol fed into the system. This equation disregards water as a reactant, although water constitutes the hydrogen source when the WGS reaction takes place. Accordingly, the hydrogen yields reported in this work might be higher than 100%.

$$MB\,(\%) = \frac{m_{out}^{liq} \bullet w_{out}^{j}}{m_{in}^{liq} \bullet w_{in}^{j}} + X \tag{8}$$

$$X\,(\%) = \frac{x_{in}^{j} - x_{out}^{j}}{x_{in}^{j}} \tag{9}$$

$$S^k\,(\%) = \frac{x_{out}^{k}}{x_{in}^{j} - x_{out}^{j}} \tag{10}$$

$$H_2\ PR = \frac{\dot{n}(H_2)}{m_{catalyst}} \tag{11}$$

$$H_2\ Eff. = \frac{\dot{n}(H_2)}{RR \bullet \dot{n}(j_{in})} \tag{12}$$

$$x^{H_2}\,(\%) = \frac{\dot{n}(H_{2out})}{\sum \dot{n}(gas_{out})} \tag{13}$$

$$Y^i\,(\%) = \frac{\dot{n}(i_{out})}{\dot{n}(j_{in})} \tag{14}$$

$$Y^k\,(\%) = \frac{x_{out}^{k}}{x_{in}^{j}} \tag{15}$$

In Eqs. 8–15, j refers to the alcohol in the aqueous solution, i refers to a gaseous product and k refers to a liquid product. The m^{liq} is the total mass of aqueous solution fed into (*in*) or collected from (*out*) the system, w^j is the mass fraction of the alcohol in the aqueous solution fed into (*in*) or collected from (*out*) the system, x is molar fraction and $\dot{n}$ is molar flow rate, and $m_{catalyst}$ is the mass of catalyst loaded into the reactor. In Eqs. 9, 10 and 15, mol fractions of liquid compounds were applied instead of molar flow rates, because the molar flow rate of the outlet liquid was unavailable due to experimental limitations to measure it accurately. Accordingly, these equations do not take into account possible changes in the total number of moles.

3. Results and discussion

3.1. Catalysts characterization

The ceria-zirconia-supported catalysts were impregnated with either nickel, or nickel and cerium or copper, and the metal content in the catalyst was determined with AAS analysis (Table 2). Compared to the targeted amounts (Table 1), about 90% of the Ni target was successfully impregnated on 17CeZr and 25CeZr supports, whereas when Cu or Ce were additionally impregnated, only about 70% of the target Ni was deposited. The mass percentage of Cu, 3.8%, was also lower than originally targeted, 5%. The amount of Ce detected in NiCe/25CeZr was affected by the cerium in the support and the impregnation efficiency cannot be evaluated in this case. The alumina-supported catalyst contained as much Ni as targeted (13%). The impregnation success on the alumina support can be attributed to its larger surface area, 159 $m^2\,g^{-1}$, compared to 17CeZr and 25CeZr supports, with 112 $m^2\,g^{-1}$ and 99 $m^2\,g^{-1}$ respectively (Table 2). The slight difference of surface area between 17CeZr and 25CeZr had no obvious effect on the amount of Ni impregnated on the catalyst.

Table 2 additionally includes the metal loadings in the spent catalysts. The APR of MeOH induced no significant change on the metal content of ceria-zirconia-supported catalysts. In the spent alumina-supported catalyst, about 30% less Ni and a 70% less Ce was observed compared to the calcined catalysts. In addition to potential leaching of Ni and Ce, the decrease of metal mass fractions can be attributed to the weight increase of the catalyst caused by the phase change to boehmite undergone by alumina (Fig. 1). The metal content of spent Cu-doped catalysts was similar to the amount in the calcined catalyst. Therefore, using Cu as a promoter improved the stability of the catalyst and prevented leaching. In contrast, during the APR of C_2 and C_3 alcohols, leaching of 20% of the Ni in Ni/17CeZr and Ni/25CeZr was observed. In a previous study [43], nickel leaching was attributed to the acidity of the reaction medium due to carbonic acid formed from CO_2. However, leaching was not observed for the most acidic feedstock applied in the present work, MeOH, which also yielded the highest amount of CO_2.

The surface area, and pore volume and average pore diameter of supports, and calcined and spent catalyst are also included in Table 2. Metal impregnation on 17CeZr and calcination decreased its surface area by 35%, whereas impregnations on 25CeZr and calcination caused a decrease between 15%–25%. The surface area of spent catalysts was generally lower than the surface area of calcined catalysts, which is attributed to partial obstruction of pores, confirmed by lower pore volume. The alumina-supported catalyst showed a considerable decrease of surface area during the APR experiments from 129 $m^2\,g^{-1}$ to 22 $m^2\,g^{-1}$. This decrease was caused by a phase change from γ-alumina to boehmite in the aqueous medium, observed in the XRD results. The structural change of the support (Fig. 1) and subsequent surface area

Table 2
Metal content determined by AAS and textural properties determined by N_2 physisorption of supports, calcined catalysts, and spent catalysts.

			AAS		N_2 physisorption		
		Ni/Cu or Ce target (mass fraction)	Ni (mass fraction)	Cu or Ce (mass fraction)	BET surface area ($m^2 \cdot g^{-1}$)	Pore Volume ($cm^3 \cdot g^{-1}$)	Average pore diameter (nm)
17CeZr	Support		n.a.	n.a.	112[c]	0.22[c]	7.0[c]
Ni/17CeZr	Calcined	10%	9.5%[c]	n.a.	73[c]	0.20[c]	8.5[c]
	MeOH		9.7%[b,c]	n.a.	72[c]	0.20[c]	8.6[c]
	EtOH		7.7%	n.a.	74	0.17	7.8
	1-PrOH		7.3%	n.a.	69	0.18	8.3
25CeZr	Support		n.a.	n.a.	99[c]	0.28[c]	10.7[c]
Ni/25CeZr	Calcined	10%	9.3%[c]	n.a.	83[c]	0.28[c]	10.9[c]
	MeOH		9.2%[c]	n.a.	76[c]	0.26[c]	11.4[c]
	EtOH		7.8%	n.a.	73	0.23	11.0
	1-PrOH		7.9%	n.a.	75	0.23	10.9
	2-PrOH		7.8%	n.a.	76	0.23	10.6
NiCu/25CeZr	Calcined	10%/5%	7.2%	3.8%	80	0.26	10.2
	MeOH		7.6%[b]	3.7%	72	0.24	11.9
	1-PrOH		6.7%	3.7%	70	0.24	11.8
	2-PrOH		8.0%[b]	4.1%[b]	71	0.24	11.8
NiCe/25CeZr	Calcined	10%/5%	7.2%	7.7%[a]	74	0.21	10.1
	MeOH		7.5%[b]	7.4%[a]	71	0.21	10.7
Al	Support		n.a.	n.a.	159[d]	0.41[d]	6.4[d]
NiCe/Al	Calcined	13%/1.3%	13.1%	2.4%[b]	129	0.32	7.4
	MeOH		9.5%	0.8%	22	0.07	9.7

n.a.: not applicable.
[a] Higher value because of the cerium in the support.
[b] Value above the amount in the calcined catalyst or the targeted amount attributed to low homogeneity of the sample or experimental error.
[c] Reported in [29].
[d] Reported in [28].

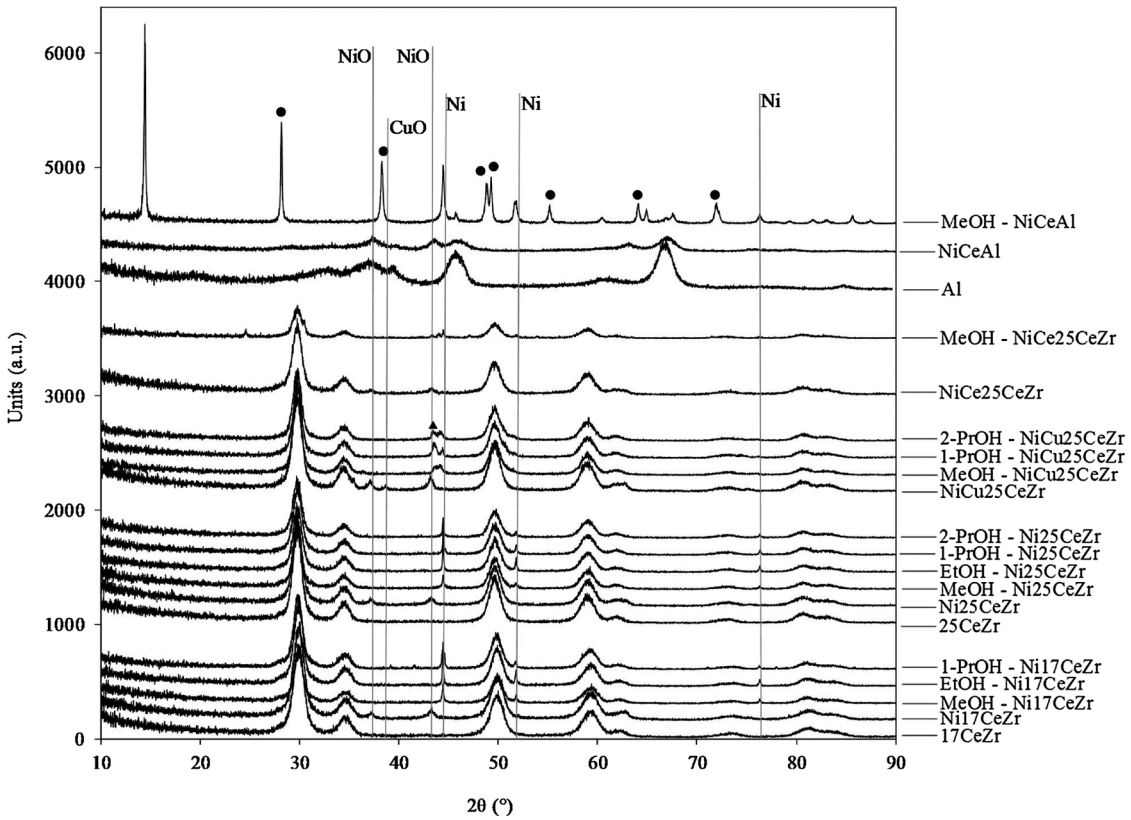

Fig. 1. X-ray diffractograms of, from bottom up, 17CeZr, calcined Ni/17CeZr and spent Ni/17CeZr catalysts; 25CeZr, calcined Ni/25CeZr and spent Ni/25CeZr catalysts; calcined NiCu/25CeZr and spent NiCu/25CeZr catalysts; calcined NiCe/25CeZr and spent NiCe/25CeZr; and Al, calcined NiCe/Al and spent NiCe/Al. NiO, CuO and Ni peaks are indicated with grey lines, Cu peaks are indicated with a triangle, and boehmite peaks are marked with spheres.

decrease may have caused metal leaching, and collapse of pores (Table 2). The surface area of CeZr-supported catalysts decreased by 4%–13% during the APR experiments; nonetheless, the type of alcohol processed had no significant effect on the surface area and pore volume of the same catalyst. The average pore size of Ni/17CeZr and Ni/25CeZr remained close to 8 nm and 11 nm respectively, during APR. The average pore diameter increased from 10 nm in calcined NiCu/25CeZr to 12 nm in the spent catalyst. The surface area of NiCe/25CeZr was 5% lower in the spent catalyst and the pore volume and average pore diameter were unaffected by the reaction conditions.

Fig. 1 presents the X-ray diffractograms of supports, calcined catalysts and spent catalysts. Compared to the pure supports, NiO peaks were identified in the X-ray diffractogram of Ni-containing catalyst at 2θ positions 36° and 43°. A CuO peak was identified for the NiCu-based catalyst at 38° 2θ. In contrast, the addition of cerium was undetected in the diffractograms of NiCe/Al and NiCe/25CeZr. After reducing the catalysts in situ, nickel remained in the metal form also after the APR experiments were carried out, regardless of the type of catalyst or feedstock applied. The diffractograms of spent catalysts presented peaks of metallic Ni at 2θ positions 44.4°, 51.9° and 77.1°. The diffractograms of spent NiCu/25CeZr additionally presented a peak at 2θ position 43.3° that corresponds to metallic Cu. Although the peaks of metallic Ni and Cu at 2θ position 44.4° and 43.3° are not completely separated, the appearance of two different peaks indicates that the complete formation of an alloy can be discarded [44]. Regarding the alumina-supported catalyst, the previously mentioned phase change from γ-alumina to boehmite (Section 3.1) is confirmed in the diffractogram of spent NiCe/Al. Boehmite can be identified in the peaks at 2θ positions 14.5°, 28.2°, 38.4°, 48.7°, 49.3°, 55.3°, 64.1° and 72.0°.

The crystallite size of Ni species in calcined catalysts and in spent catalysts determined by Scherrer equation are presented in Table 3. For the calcined catalysts, the most intense characteristic peak of NiO, 43.3° 2θ, was considered to determine its crystallite size. The peak at 44.4° 2θ, characteristic of metallic Ni, was considered for the spent catalysts. NiO crystallite size on the CeZr-supported calcined catalysts was approximately 20 nm, except for NiCe/25CeZr where larger particles were determined (28 nm). NiO crystallite size was 8 nm in the calcined NiCe/Al catalyst. APR caused no obvious effect on the nickel crystallite size of NiCu/25CeZr regardless of the feedstock applied. Accordingly, Cu promoted the stability of the catalyst, which was also indicated by the results included in Table 2. APR over the other catalysts caused different changes in the crystallite size when different feeds were processed. The APR of ethanol induced a significant growth of nickel particles in Ni/17CeZr and Ni/25CeZr. A similar effect has been described in APR over a ruthenium-based catalyst, whose metal dispersion decreased from 25% to 19% attributed to metal sintering in the APR of ethanol [19]. Moreover, a significant increase in the size of Ni particles was observed in Ni/17CeZr after the APR of methanol was conducted. As indicated in the footnote of Table 3, the Ni particle size of spent Ni/17CeZr and Ni/25CeZr was determined after the catalysts had been 12 h on stream and had been reduced twice. Accordingly, Ni/17CeZr has lower tolerance to the reduction and APR conditions that caused the increase of Ni particles compared to Ni/25CeZr. On the other hand, the alumina supported catalyst suffered obvious Ni agglomeration in the APR of MeOH due to the phase change to boehmite.

Table 3
Crystallite size of NiO in calcined catalysts and Ni in spent catalyst, determined from XRD with the Scherrer equation.

Catalyst	Crystallite size of nickel species (nm)				
	Calcined catalyst d_{NiO}	Spent catalyst d_{Ni}			
		MeOH	EtOH	1-PrOH	2-PrOH
Ni/17Ce-Zr	21	43[a]	75	25	n.a.
Ni/25Ce-Zr	20	23[a]	71	47	55
NiCu/25CeZr	21	17	n.a.	22	19
NiCe/25CeZr	28	49	n.a.	n.a.	n.a.
NiCe/Al	8	31	n.a.	n.a.	n.a.

n.a.: not applicable.
[a] Re-reduction after 6 h on stream and total time on stream of 12 h.

3.2. Reactivity of C_1-C_3 alcohols

To maximize the H_2 production was one of the main targets of this work. Hydrogen constituted the main gaseous product in the APR of C_1-C_3 alcohols over different catalysts, with H_2 molar fraction in the gas phase between 63% and 95% (Table 4). Hydrogen production and yield are useful parameters to evaluate the overall amount of hydrogen produced in the APR process independent of the reaction pathways. In the APR of MeOH, the highest values of H_2 production rate were reached, between (1.9–2.4) $mmol \cdot min^{-1} \cdot g_{catalyst}^{-1}$, and H_2 yields, between 93% and 110% over Ni/17CeZr, Ni/25CeZr and NiCu/25CeZr. In contrast, NiCe/25CeZr and NiCe/Al exhibited poorer performance with 70% lower hydrogen production rate and yield. The APR of other alcohols produced different amounts of H_2 depending on the catalyst. Over Ni/17CeZr, the hydrogen production and yield were higher in the APR of EtOH than in the APR of 1-PrOH. Similarly, the APR of 1-PrOH resulted in lower amounts of hydrogen over NiCu/25CeZr, in this case, compared to the amount obtained from 2-PrOH. The lowest amounts of hydrogen were obtained from the APR of 1-PrOH over Ni/17CeZr, 0.27 $mmol \cdot min^{-1} \cdot g_{catalyst}^{-1}$ and 24% H_2 yield, and over NiCu/25CeZr with 0.15 $mmol \cdot min^{-1} \cdot g_{catalyst}^{-1}$ of H_2 and 13% H_2 yield, and from the APR of EtOH over Ni/25CeZr 0.25 $mmol \cdot min^{-1} \cdot g_{catalyst}^{-1}$ of H_2 and 17% H_2 yield. Over Ni/25CeZr and NiCu/25CeZr, H_2 was produced in similar amounts in the APR of 2-PrOH, (0.45 and 0.50) $mmol \cdot min^{-1} \cdot g_{catalyst}^{-1}$, and 41% and 45% H_2 yield respectively.

H_2 efficiency indicates the extent of full reforming to gases and WGS (Eq. 1–4 and 5, Section 2.3). Those alcohols whose reaction pathway in APR was mainly full reforming to gases and subsequent WGS will show higher H_2 efficiency. The APR of MeOH produced only gases regardless of the catalyst applied. In the APR of MeOH, H_2 efficiency values were around 35% over Ni/17CeZr, Ni/25CeZr and NiCu/25CeZr. It is worth noticing that NiCu/25CeZr was able to reach a H_2 efficiency similar to Ni/17CeZ and Ni/25CeZr with 20% lower MeOH conversion. The APR of MeOH over NiCe/25CeZr and NiCe/Al resulted in low conversions, around 15%, with similarly low H_2 efficiency, below 10%. In the APR of C_2-C_3 alcohols, different reaction pathways to full reforming and WGS to produce H_2, and side reactions that consume H_2 explain considerably lower H_2 efficiency.

Mainly gaseous products were obtained also in the APR of EtOH over Ni/17CeZr and Ni/25CeZr. However, 30% selectivity to liquid products indicates that full conversion to gases and WGS (Eqs. 2 and 5) were not the only reaction pathways, and side reactions to produce ethanal took additionally place. Ni/17CeZr and Ni/25CeZr reached also similar conversions close to 15%. However, H_2 efficiency over Ni/17CeZr, 7%, was more than twice the value achieved over Ni/25CeZr, which suggest higher selectivity to the full reforming and WGS pathway (Eqs. 2 and 5) over Ni/17CeZr.

The APR of 1-PrOH resulted in liquid product selectivities around 25%, over Ni/17CeZr, Ni/25CeZr and NiCu/25CeZr. Therefore, as in the APR of EtOH, full conversion to gases and WGS (Eqs. 3 and 5) was not the only reaction pathway and side reactions to produce liquid compounds took additionally place. The conversion of 1-PrOH over Ni/25CeZr, 44%, was twice as high as over NiCu/25CeZr, and three times as high as over Ni/17CeZr. H_2 efficiency was the highest over Ni/25CeZr, 7%, which suggest relatively higher selectivity to the reaction pathway that involves full reforming to gases and WGS (Eqs. 3 and 5). Over Ni/17CeZr and NiCu/25CeZr, the APR of 1-PrOH resulted in lower H_2 efficiency around 3% and 1% respectively.

In the APR of 2-PrOH, similar results were obtained over Ni/25CeZr

Table 4
Results of the APR of different feeds over nickel-based catalysts.

Catalyst	Feed	Feed molar flow rate (mmol·min^{-1})	t + 1 (°C)	MB[b]	X[b]	Liq. S[b]	H_2 PR[b] (mmol·min^{-1}· $g_{catalyst}^{-1}$)	H_2 Y[b]	x^{H2}, [b]	H_2 Eff.[b]
Ni/17CeZr	MeOH	3.1	230[a]	96%	51%[a]	0	1.9	93%	79%	31%
	EtOH	2.2	232	98%	12%	32%	0.62	42%	77%	7%
	1-PrOH	1.7	235	n.a.	15%	30%	0.27	24%	65%	3%
Ni/25CeZr	MeOH	3.1	230[a]	98%	59%[a]	0	2.4	110%	73%	37%
	EtOH	2.2	233	91%	15%	28%	0.25	17%	63%	3%
	1-PrOH	1.7	235	96%	44%	24%	0.66	59%	66%	7%
	2-PrOH	1.7	231	98%	56%	63%	0.45	41%	88%	4%
NiCu/25CeZr	MeOH	3.1	233	97%	38%	0	2.1	101%	76%	34%
	1-PrOH	1.7	230	102%	22%	25%	0.15	13%	85%	1%
	2-PrOH	1.7	230	93%	59%	69%	0.50	45%	95%	5%
NiCe/25CeZr	MeOH	3.1	230	97%	12%	0	0.62	18%	77%	6%
NiCe/Al	MeOH	3.1	230	98%	19%	0	0.95	28%	82%	9%

n.a. not available.
[a] Reported in [29].
[b] MB: mass balance (Eq. 8), X: conversion (Eq. 9), Liq. S: selectivity to liquids (Eq. 10), H_2 PR: hydrogen production rate (Eq. 11), H_2 Y: hydrogen yield (Eq. 14), x^{H2}: hydrogen molar fraction among gaseous products (Eq. 13), H_2 Eff.: hydrogen efficiency (Eq. 12).

and NiCu/25CeZr differing from the APR of other alcohols in the liquid selectivity. The APR of 2-PrOH resulted in higher liquid product selectivity around 65% and its conversion was comparable to that achieved in the APR of MeOH, close to 60%. However, H_2 efficiency was relatively low, 5%. High selectivity to liquids and low H_2 efficiency with high conversion indicates that 2-PrOH was converted and H_2 was produced through a reaction pathway different to full reforming to gases and WGS (Eqs. 4 and 5).

The discussion included in the previous paragraphs suggests that the APR reaction pathway of C_1-C_3 is more complex than that explained by Eqs. 1–5. Therefore, the following subsections will be devoted to the evaluation of the product distribution obtained in the APR of C_1-C_3 over different catalysts to achieve a better understanding of the reaction pathways in the APR.

3.2.1. The effect of dopants on the catalyst performance in the APR of MeOH

The APR of MeOH over different Ni-based, and Cu- and Ce-containing catalysts was conducted to evaluate the effect of metal dopants on the catalyst performance. Methanol conversion and H_2 yield decreased in the order Ni/25CeZr > NiCu/25CeZr > NiCe/Al > NiCe/25CeZr (Table 4 and Fig. 2). Both Ce-doped catalysts, NiCe/25CeZr and NiCe/Al, showed significantly poorer performance than the other catalysts. The H_2 yield over the Ce-doped catalysts was less than 40% of the H_2 yield over Ni/25CeZr (Table 4 and Fig. 2). The lower performance of NiCe/Al catalyst can be attributed to the phase change undergone by γ-Al_2O_3 to boehmite and consequent decrease in the surface area, and metal agglomeration and leaching (Section 3.1). The results obtained over NiCe/25CeZr are surprisingly poor compared to those obtained over similar catalysts such as Ni/25CeZr or NiCu/25CeZr. The poorer results over NiCe/25CeZr reveal the negative effect of nickel particle growth (Table 3) on the performance of this catalyst, compared to the other 25CeZr-supported catalysts. Over NiCu/25CeZr, the MeOH conversion was lower than over Ni/25CeZr, and the H_2 yields were similar over NiCu and Ni on 25CeZr, which explains the higher H_2 molar fraction among gases over the Cu-doped catalyst (Table 4), as similarly reported in [29]. In addition, the product distribution was similar over Ni/25CeZr and NiCu/25CeZr (Fig. 2). The presence of CO_2 among the gases confirms WGS reaction activity (Eq. 5) over both catalysts. The detected CH_4 indicates that methanation of carbon oxides with hydrogen consumption took place, also observed over NiCe/25CeZr. Conversely, the only products observed over NiCe/Al were H_2 and CO_2, which indicates that CO conversion through the WGS reaction (Eq. 5) was highly promoted. No side products over NiCe/Al suggest that the selectivity was superior to that over the other Ce-doped catalyst, NiCe/25CeZr. Lower conversion over NiCe/Al hinders the comparison in terms of selectivity with the other 25CeZr-supported catalysts.

The yields obtained over NiCu/25CeZr, compared to that of Ni/25CeZr, suggest that copper addition promoted the WGS reaction and methanation was less favourable. Additionally, MeOH conversion was lower over NiCu/25CeZr than over Ni/25CeZr. To evaluate the effect of

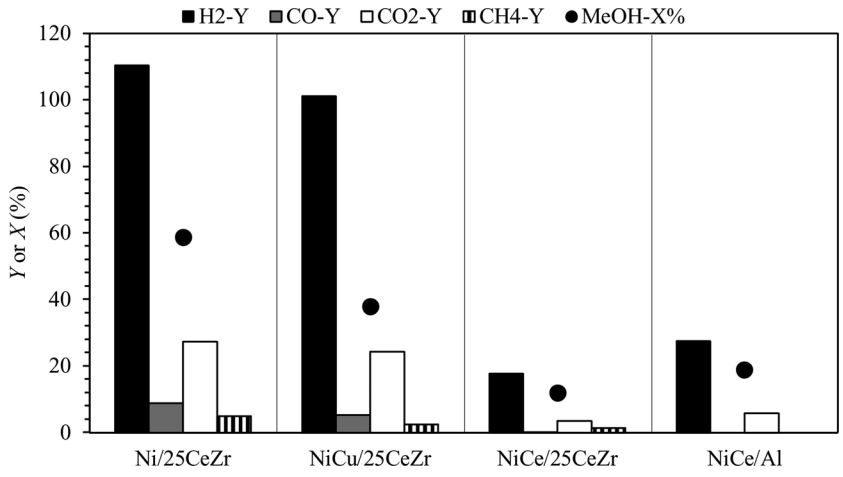

Fig. 2. Methanol conversions (dots) and yields (columns) of hydrogen (black), carbon monoxide (grey), carbon dioxide (white), and methane (vertical lines) in APR over Ni/25CeZr [29] and doped, Ni-based catalysts.

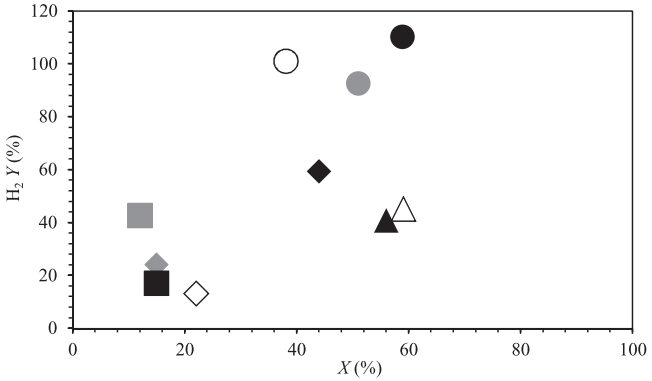

Fig. 3. Hydrogen yield (H_2 Y) versus conversion (X) of MeOH (sphere), EtOH (cube), 1-PrOH (diamond) and 2-PrOH (triangle) over Ni/17CeZr (grey), Ni/25CeZr (black) and NiCu/25CeZr (white).

Ni content on the APR of MeOH, the Ni loading was used to calculate the H_2 production rate per mass of Ni using the values of H_2 production rate in Table 4. Ni/25CeZr had a Ni loading of 9% mass fraction whereas NiCu/25CeZr had 7% mass fraction of Ni (Table 2). Accordingly, the H_2 production rate was 27 mmol·min^{-1}· g_{Ni} $^{-1}$ over Ni/25CeZr and 30 mmol·min^{-1}· g_{Ni} $^{-1}$ over NiCu/25CeZr. These Ni-based H_2 production rate indicates that lower H_2 production rate over NiCu/25CeZr (Table 4) could be attributed to its lower amount of Ni compared to Ni/25CeZr; moreover, a possible negative effect of Cu on MeOH reforming could also explain it.

3.2.2. *The effect of feedstock and catalyst on H_2 yield and conversion of C_1-C_3 alcohols*

Methanol is a simple molecule with no C—C bonds, and a C/O stoichiometry of 1:1 that allows high selectivity towards hydrogen in APR [45]. Accordingly, the APR of methanol resulted in high conversions and hydrogen yields. However, longer chain alcohols present C—C bonds and different C/O stoichiometry, which, along with the catalyst, has a noticeable effect on the alcohols conversion and H_2 yield (Table 4 and Fig. 3). Fig. 3 summarizes the hydrogen yield versus alcohol conversion obtained in the APR of C_1-C_3 alcohols over different catalyst (data from Table 4).

Conversion and H_2 yield were the highest over Ni/25CeZr (Fig. 3, black) when MeOH and 1-PrOH were applied. In contrast, the APR of 2-PrOH over NiCu/25CeZr (Fig. 3, white) resulted in slightly higher conversion, and in the APR of EtOH, a noticeably higher yield was reached over Ni/17CeZr (Fig. 3, grey). Alcohol conversion and H_2 yield in the APR of EtOH and 1-PrOH followed different trends over different catalysts.

MeOH (Fig. 3, spheres) was converted more easily into H_2 than longer-chain alcohols, although the number of hydrogen atoms contained in MeOH is lower. Conversion of 2-PrOH (Fig. 3, triangles) achieved the level of MeOH conversions; however, the H_2 yields were considerably lower. The conversion of EtOH (Fig. 3, cubes) was significantly lower than the conversion of the other alcohols and similar over Ni/17CeZr and Ni/25CeZr. The APR of EtOH caused the agglomeration of Ni particles in both catalysts (Table 3), which decreased the number of active sites and likely resulted in lower conversions. H_2 yield in the APR of EtOH was higher over Ni/17CeZr than over Ni/25CeZr. The conversion of specially 1-PrOH (Fig. 3, diamonds) varied considerably over different catalysts. The alcohol was converted to a larger extent and resulted in higher H_2 yield over Ni/25CeZr than over Ni/17CeZr. Accordingly, higher amount of Ce in the support could have resulted in higher catalytic activity in this case.

3.2.3. *Product distribution and reaction pathways from C_1-C_3 alcohols*

The main reaction pathways in the APR of MeOH can be deduced from the product distribution (Figs. 2 and 4). Methanol is accompanied by longer-chain alcohols in real water fractions derived from FT synthesis. Therefore, the product distribution from the APR of C_2 and C_3 alcohols was additionally studied to understand the effect of C—C bonds, higher C/O ratio and higher number of hydrogen atoms in the alcohols on the product distribution. The effect of the hydroxyl group location in C_3 alcohols on the bond scissions and consequent product distribution was also addressed. The product distribution derived from the APR of C_2 and C_3 alcohols was evaluated to enhance the understanding of the reaction pathways in APR of different alcohols over different catalysts. Fig. 4 shows the conversion of different alcohols and product yields over three different catalysts. The information presented

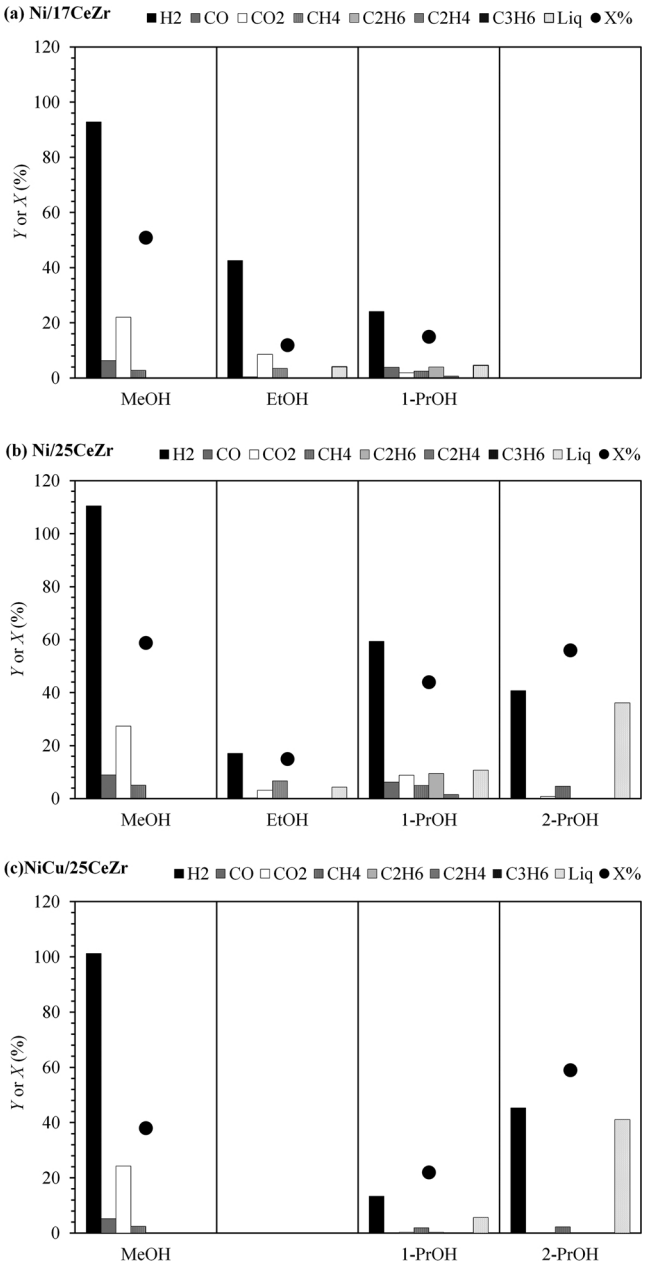

Fig. 4. Alcohol conversions (dots) and yields (columns) of H_2 (black), CO (dark grey), CO_2 (white), methane (vertical lines), ethane (light grey), ethylene (diagonal lines), propene (black with white dots), and liquid products (white with black dots) in the APR of different alcohols over Ni/17CeZr (a) Ni/25CeZr (b), and NiCu/25CeZr (c). The liquid products were ethanal from EtOH, sum of propanal and negligible amounts of propionic acid from 1-PrOH, and acetone from 2-PrOH.

in Fig. 4 will be discussed in this section to propose potential reaction pathways followed by different C_1-C_3 alcohols in APR over Ni/17CeZr, Ni/25CeZr and NiCu/25CeZr.

The APR of MeOH produces H_2 and CO (Eq. 1). Moreover, CO_2 is produced through WGS reaction (Eq. 5), which decreases the amount of CO while favouring the H_2 yield (Fig. 4). In addition, CH_4 produced in methanation (Eqs. 6 and 7), was identified among the products from APR of MeOH over the three catalysts, Ni/17CeZr, Ni/25CeZr and NiCu/25CeZr. Ethane and propene were detected in negligible amounts over the monometallic catalysts. Undesired alkane formation was restricted over NiCu/25CeZr, which resulted in lower amounts of methane. Furthermore, no liquid products were detected in the liquid samples from the APR of MeOH over either of the catalysts.

In the APR of EtOH, H_2, CH_4 and CO_2 were the main gaseous products, in addition to negligible amounts of C_2H_6 and C_3H_6, and ethanal was the only liquid product (Fig. 4 a and b). Ni/17CeZr produced considerably larger amounts of hydrogen with similar conversion to that achieved over Ni/25CeZr. The difference in the H_2 yields suggests that the APR of EtOH followed different pathways over Ni/17CeZr and Ni/25CeZr, which is also indicated by the different formation ratio of CO_2 and CH_4. Large amounts of H_2 can be produced via full reforming of EtOH to gases and WGS (Eqs. 2 and 5). Additionally, H_2 can be produced through EtOH dehydrogenation (Eq. 16) or decarbonylation (Eq. 18).

Ethanol dehydrogenation

$$C_2H_5OH\ (l) \overset{H_2O}{\longleftrightarrow} C_2H_4O\ (l) + H_2\ (g) \qquad \Delta G_{503} = +21.6\,kJ \tag{16}$$

Ethanal decarbonylation

$$C_2H_4O\ (l) \overset{H_2O}{\longleftrightarrow} CO\ (g) + CH_4\ (g) \qquad \Delta G_{503} = -95.2\,kJ \tag{17}$$

Ethanol decarbonylation

$$C_2H_5OH\ (l) \overset{H_2O}{\longleftrightarrow} CH_4\ (g) + CO\ (g) + H_2\ (g) \qquad \Delta G_{503} = -73.6\,kJ \tag{18}$$

In the dehydrogenation of EtOH, ethanal is formed, as previously suggested in a different study [46], whereas the decarbonylation of EtOH involves the formation of CH_4 and CO, as proposed in [47]. Ethanal yield was low and similar over Ni/17CeZr and Ni/25CeZr, which indicates that EtOH dehydrogenation was low regardless of the catalyst. The formation of ethanal is thermodynamically unfavourable (Eq. 16), and thus, ethanal yields were low. EtOH decarbonylation (Eq. 18) was more thermodynamically favourable, also compared to full EtOH reforming to gases (Eq. 2). However, considering the stoichiometry of Eqs. 2 and 18 and the product distribution in Fig. 4 a and b, it can be assumed that additionally, full reforming to gases took place over Ni/17CeZr and Ni/25CeZr because the H_2 yield was higher than that of CO and CH_4. Nevertheless, full reforming to gases was more favourable over Ni/17CeZr according to the significantly higher H_2 yield and lower CH_4 yield compared to Ni/25CeZr.

The formation of CH_4 and CO can take place via three different pathways in the APR of EtOH: (i) ethanal decarbonylation (Eq. 17); (ii) EtOH decarbonylation (Eq. 18), which also produces H_2 as previously indicated; and (iii) EtOH full reforming to CO and H_2 (Eq. 2) followed by hydrogenation of carbon oxides into CH_4 (Eqs. 6 and 7). Considering the stoichiometry of Eqs. 2,17 and 18, the product distribution obtained in the APR of EtOH (Fig. 4) suggests that EtOH decarbonylation (Eq. 18) was more favourable over Ni/25CeZr than over Ni/17CeZr. This reaction pathway (Eq. 18) explains the lower H_2 and CO_2 yields and larger amount of CH_4 over Ni/25CeZr compared to the product distribution obtained over Ni/17CeZr, where full reforming was more favoured. Furthermore, similarly negligible CO yields over Ni/17CeZr and Ni/25CeZr indicate that CO_2 is formed via WGS reaction (Eq. 5), which allows the formation of additional H_2.

The APR of 1-PrOH was conducted over Ni/17CeZr, Ni/25CeZr and NiCu/25CeZr. Hydrogen was the main product over these three catalysts. Over NiCu/25CeZr, CH_4 was also formed, whereas over Ni/17CeZr and Ni/25CeZr, CO, CO_2, C_2H_6 and a small amount of C_2H_4 were additionally observed. The main liquid product detected over the three catalysts was propanal (Fig. 4). Hydrogen yield was higher over Ni/25CeZr than over Ni/17CeZr due to higher 1-PrOH conversion. On the other hand, although Ni/17CeZr and NiCu/25CeZr allowed similar 1-PrOH conversions, the H_2 yield was higher over Ni/17CeZr. The differences in the H_2 yield suggest that 1-PrOH followed different reforming pathways over different catalysts, which is also indicated by the different formation ratio of CO_2 and CH_4 (Fig. 4).

Hydrogen can be produced via full reforming of 1-PrOH to gases and WGS (Eqs. 3 and 5). Additionally, H_2 can be produced through 1-PrOH dehydrogenation (Eq. 19) or decarbonylation (Eq. 21) [48]. In the dehydrogenation of 1-PrOH, propanal is formed, whereas the decarbonylation of 1-PrOH involves the formation of C_2H_4 and CO, as proposed in Ref. [47]. Propanal yield was low and similar over Ni/17CeZr and NiCu/25CeZr, and slightly higher over Ni/25CeZr due to higher conversion. Thus, 1-PrOH dehydrogenation (Eq. 19) took place at a relatively low extent regardless of the catalyst. Nonetheless, the reaction stoichiometry of Eq. 19 matches the product distribution obtained over NiCu/25CeZr. In contrast, the product distribution obtained over Ni/17CeZr and Ni/25CeZr indicates that full reforming of 1-PrOH to gases and WGS (Eqs. 3 and 5) was the main reaction pathway to produce hydrogen, which was obtained in significantly larger amounts than the other products.

Propan-1-ol dehydrogenation

$$C_3H_7OH\ (l) \overset{H_2O}{\longleftrightarrow} C_3H_6O\ (l) + H_2\ (g) \qquad \Delta G_{503} = +9{,}5\,kJ \tag{19}$$

Propanal decarbonylation

$$C_3H_6O\ (l) \overset{H_2O}{\longleftrightarrow} C_2H_6\ (g) + CO\ (g) \qquad \Delta G_{503} = -82.7\,kJ \tag{20}$$

Propan-1-ol decarbonylation

$$C_3H_7OH\ (l) \overset{H_2O}{\longleftrightarrow} C_2H_4\ (g) + CO\ (g) + 2H_2\ (g) \qquad \Delta G_{503} = +1.3\,kJ \tag{21}$$

Over Ni/17CeZr, C_2H_6 was produced in stoichiometric amounts with CO, in agreement with Eq. 20. An additional source of CO could have been the 1-PrOH decarbonylation (Eq. 21) accompanied by the production of C_2H_4 and H_2. However, low C_2H_4 yield indicates that this reaction did not take place to a significant extent over Ni/17CeZr. CO_2 and CH_4 resulted from the WGS reaction (Eq. 5) and methanation of carbon oxides (Eqs. 6 and 7) respectively. However, CO_2 and CH_4 low yields suggest that WGS and methanation were less favoured. Over Ni/25CeZr, C_2H_6 was also produced accompanied by CO via propanal decarbonylation (Eq. 20). Carbon monoxide might have been also formed in the 1-PrOH decarbonylation (Eq. 21), which explains the production of C_2H_4 and additional H_2. Higher CO_2 yield than CO over Ni/25CeZr indicates that WGS (Eq. 5) was more favourable than over Ni/17CeZr. The presence of CH_4 in the gases indicates that methanation of oxides (Eqs. 6 and 7) took also place over Ni/25CeZr.

Carbon monoxide was not detected in the APR of 1-PrOH over NiCu/25CeZr and CO_2, C_2H_6 and C_2H_4 were observed in negligible amounts. The presence of CH_4 in the gas stream obtained over NiCu/25CeZr suggests that hydrogenation of carbon oxides took place (Eqs. 6 and 7). Accordingly, we conclude that NiCu/25CeZr mainly follows the reaction pathway in Eq. 19, which has been previously suggested by Lei et al. [24]. However, that suggestion differs from the observation by Wawrzetz et al. [23], who stated that decarboxylation of propionic acid to C_2H_6 and CO_2 was the main reaction after formation of propanal from 1-PrOH.

The conversion and product distribution in the APR of 2-PrOH was similar over Ni/25CeZr and NiCu/25CeZr (Fig. 4 b and c). Considering the main reaction products, acetone and H_2, 2-PrOH dehydrogenation to the ketone (Eq. 22) was assumed to be the predominant reaction pathway, which has been previously proposed in [47]. Further reaction

of acetone through decarbonylation (Eq. 23) results in CH_4 and CO. As observed in Fig. 4 b and c, decarbonylation of acetone was limited over both catalysts. Nonetheless, higher acetone decarbonylation over Ni/25CeZr slightly lowered the H_2 yield and increased the amount of CH_4 among the products.

Propan-2-ol dehydrogenation

$$C_3H_7OH\,(l) \overset{H_2O}{\longleftrightarrow} C_3H_6O\,(l) + H_2\,(g) \qquad \Delta G_{503} = -12.4\,kJ \tag{22}$$

Acetone decarbonylation

$$C_3H_6O\,(l) + H_2\,(g) \overset{H_2O}{\longleftrightarrow} 2CH_4\,(g) + CO\,(g) \qquad \Delta G_{503} = -119.2\,kJ \tag{23}$$

In a different study [23] on the APR of 2-PrOH over Pt/Al_2O_3, acetone has been reported to be the only product and no H_2 had been observed, in contract to the present work. No CO was detected among the gaseous products resulting from the APR of 2-PrOH (Fig. 4 b and c). This suggest CO conversion to CO_2 through WGS reaction (Eq. 5), or hydrogenation of CO, and also CO_2, to form CH_4 (Eqs. 6 and 7) might have taken place under the reaction conditions. Negligible amounts of C_2H_6 and C_3H_6 were additionally detected.

3.2.4. Bond cleavage of C_1-C_3 alcohols

The product distribution in the APR of different alcohols originates from the C—H and O—H bond cleavage of those bonds adjacent to the —CO— functional group [46]. For MeOH, the cleavage of these bonds led to full reforming to gases according to the thermodynamically favourable Eq. 1 with negative Gibbs free energy. For the longer-chain alcohols, Gibbs free energies of full reforming to gases (Eqs. 2–4) have positive values. Therefore, full reforming of EtOH, 1-PrOH and 2-PrOH to gases was expected to happen to a lesser extent than from MeOH. Fig. 5 shows the main reaction pathways proposed for the APR of MeOH, EtOH, 1-PrOH and 2-PrOH.

The APR of MeOH proceeds through O—H and C—H bonds scission (Fig. 5 a). First the O—H bond cleaves resulting in the formation of methoxy intermediates before decomposition to CO and H_2 [46]. Every hydrogen atom in MeOH is activated to produce molecular hydrogen, which explains the high H_2 yield reached in the APR of MeOH (Table 4 and Fig. 4). To maximize the H_2 production, CO should be converted in the WGS reaction (Eq. 5) and limit C—O bond cleavage that takes place in side reactions, such as methanation, where H_2 is consumed to produce methane (Eqs. 6 and 7). NiCu/25CeZr successfully limited C—O bonds scission in the APR of MeOH.

The APR of EtOH proceeds through O—H and C—H, and C—C bonds scission when full reforming to gases and decarbonylation reactions take place (Fig. 5b). The experimental results elucidated that the reaction pathways followed by EtOH in APR appear to be different over Ni/17CeZr and Ni/25CeZr. The product distribution obtained over Ni/17CeZr suggests that full reforming to gases (Eq. 2) was dominant in accordance with the larger H_2 yield obtained. Lower H_2 yield and relatively significant amounts of CH_4 suggest that EtOH decarbonylation was more favourable over Ni/25CeZr. Accordingly, the cleavage of multiple C—H bonds from the alkyl group was more favourable over Ni/17CeZr. When only O—H and C—H bonds cleave in EtOH, ethanal was formed. The ethanal formation pathway via alcohol dehydrogenation (Eq. 16) was less favourable than the gas formation that involved C—C bond cleavage over both Ni/17CeZr and Ni/25CeZr (Eqs. 2 and 18), in agreement with the negative reaction Gibbs free energy changes and the obtained product distributions (Fig. 4).

Full reforming of 1-PrOH to gases (Eq. 3) was less thermodynamically favourable than the dehydrogenation or decarbonylation of the alcohol (Eqs. 19 and 21). However, the experimental results indicates that the APR of 1-PrOH proceeds through O—H and C—H, and C—C bonds scission when full reforming and decarbonylation reactions took place (Fig. 5 c). These pathways were the most favourable over Ni/17CeZr and Ni/25CeZr. However, conversely to the APR of EtOH, full reforming and the cleavage of multiple C—H bonds in the alkyl group were more favourable over Ni/25CeZr. When only O—H and C—H bonds cleave in 1-PrOH, propanal was formed. This reaction pathway was less favourable over Ni/17CeZr and Ni/25CeZr. In contrast, propanal formation was the preferred reaction pathway over NiCu/25CeZr. These results over NiCu/25CeZr confirm that full reforming to gases was inhibited in the APR of 1-PrOH by the addition of Cu to the catalyst.

The APR of 2-PrOH mainly proceeds through C—H and O—H bond

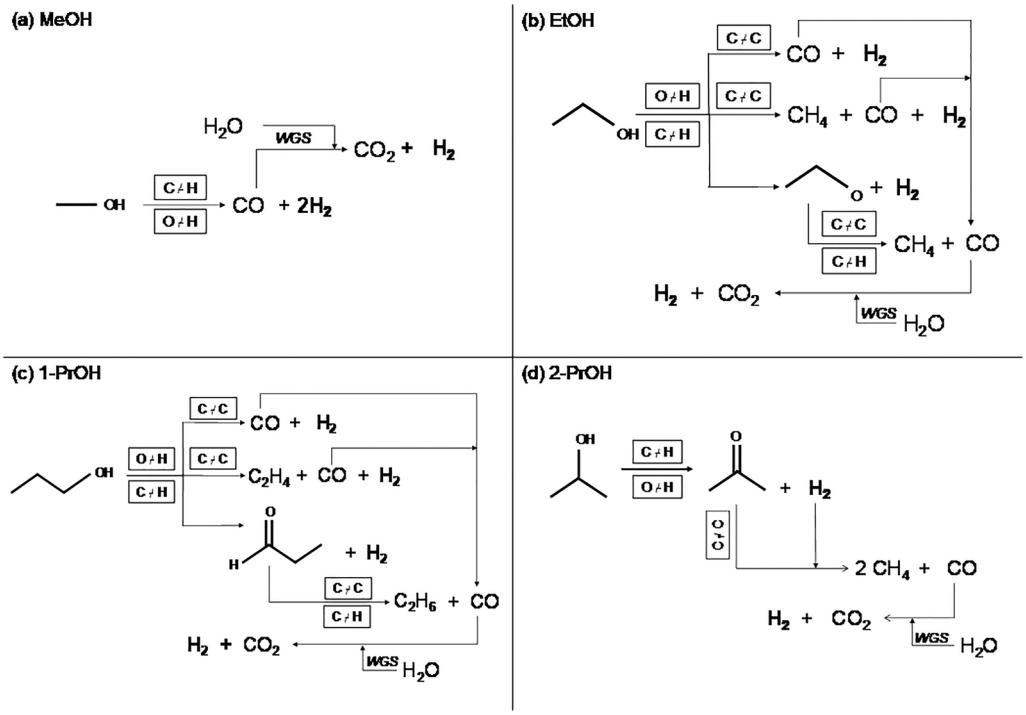

Fig. 5. Summary of the proposed reaction pathways and main bond cleavages.

cleavage to form acetone (Fig. 5 d) over Ni/25CeZr and NiCu/25CeZr. Therefore, 2-PrOH dehydrogenation was the main reaction pathway in agreement with the spontaneous Gibbs free energy of Eq. 22. The C—C and C—H bond cleavages involved in full reforming to gases (Eq. 4) were unfavourable. Further C—C of acetone to CH_4 and CO was neither a significant pathway. However, this reaction pathway took place to a larger extent over Ni/25CeZr than over NiCu/25CeZr.

4. Conclusions

Catalytic APR of C_1-C_3 alcohols was conducted over different nickel-based catalysts. The results of these experiments allowed the evaluation of the product distribution to propose potential reaction pathways followed by different alcohols in APR over nickel-based catalyst. In addition, Cu and Ce were used as dopants to assess their effect on the performance and stability of ceria-zirconia and alumina supported catalysts. The addition of Cu to the Ni-based 25CeZr-supported catalyst promoted the catalyst stability and more selective production of H_2. The addition of Ce to the Ni-based 25CeZr-supported catalyst adversely affected the catalyst stability and activity. The other Ce-doped catalyst, NiCe/Al, promoted CO-free hydrogen production, and the undesired formation of CH_4 was prevented in the APR of MeOH.

Focusing on Ni/17CeZr, Ni/25CeZr and NiCu/25CeZr, these catalysts performed differently in the APR of C_1-C_3 alcohols. The suggested reaction pathways in the APR of C_2–C_3 alcohols comprises full reforming to gases, and alcohol dehydrogenation and decarbonylation. The extent in which these reactions took place depended on the type of feedstock and catalyst. In the APR of MeOH, H_2 yield was high due to high MeOH conversion via full reforming to gases and the subsequent WGS reaction. Larger amounts of ceria in the support allowed a higher MeOH conversion, and Cu-doping limited CH_4 formation. In the APR of longer-chain alcohols, Ni/17CeZr and Ni/25CeZr were active in the cleavage of O—H, C—H and C—C bonds for full reforming to gases. However, side reactions such as alcohol dehydrogenation and decarbonylation were significant. Over NiCu/25CeZr, C_2-C_3 alcohols mainly followed the dehydrogenation pathway. Thus, Cu restricted the full reforming of alcohols to gases due to lower activity in the C—C bond cleavage, which limited the H_2 yield.

Ni/17CeZr, Ni/25CeZr and NiCu/25CeZr are potential catalysts to process the oxygenated hydrocarbons in FT-derived water fractions. The monometallic Ni/17CeZr and Ni/25CeZr are preferred to maximize the hydrogen production. Nonetheless, NiCu/25CeZr could be additionally considered because of its improved stability during the experiments, compared to the monometallic catalyst, and when more selective production of hydrogen among gases is required.

Acknowledgements

The authors thank Dr. Pekka Simell, Prof. Klaus Hellgardt and Prof. Leon Lefferts for their guidance and support. We are grateful to Aleksi Rinta-Paavola for his help with the preparation and characterization of catalysts, to Tyko Viertiö and Eveliina Mäkelä for their help with the adsorption isotherm measurements, and to Laura Lonka for her help with the APR experiments. The Bioeconomy Infrastructure and the Raw materials research infrastructure (RAMI) that permitted conducting the experimental work for this study at both VTT and Aalto University. This work was funded by Academy of Finland (AQUACAT Project no. 285398).

References

[1] R.J.J. Nel, A. De Klerk, Ind. Eng. Chem. Res. 46 (2007) 3558–3565.
[2] R.D. Cortright, 2005 IEEE Veh. Power Propuls. Conf. VPPC, (2005), pp. 492–494.
[3] I. Coronado, M. Stekrova, M. Reinikainen, P. Simell, L. Lefferts, J. Lehtonen, Int. J. Hydrogen Energy 41 (2016) 11003–11032.
[4] R.R. Davda, J.W. Shabaker, G.W. Huber, R.D. Cortright, J.A. Dumesic, Appl. Catal. B Environ. 43 (2003) 13–26.
[5] M. Martín, I.E. Grossmann, Ind. Eng. Chem. Res. 53 (2014) 7730–7745.
[6] H.A. Duarte, M.E. Sad, C.R. Apesteguía, Catal. Today 296 (2017) 59–65.
[7] L.A. Dosso, C.R. Vera, J.M. Grau, Int. J. Hydrogen Energy 42 (2017) 18853–18864.
[8] M. El Doukkali, A. Iriondo, N. Miletic, J.F. Cambra, P.L. Arias, Int. J. Hydrogen Energy 42 (2017) 23617–23630.
[9] L.P.F. Dancuart Kohler, G.H. Du Plessis, F.J. Du Toit, E.L. Koper, T.D. Phillips, J. Van Der Walt, (2003), Method of Purifying Fischer-Tropsch Derived Water, WO 03/106349 A1, n.d.
[10] D.J. Clur, G.D.H. Shaw, (2005), Recovery of Water Originating from Low Temperature Fischer-Tropsch Synthesis Processes, WO 2005/113426 A1, n.d.
[11] J.W. Shabaker, R.R. Davda, G.W. Huber, R.D. Cortright, J.A. Dumesic, J. Catal. 215 (2003) 344–352.
[12] Z. Tang, J. Monroe, J. Dong, T. Nenoff, D. Weinkauf, Ind. Eng. Chem. Res. 48 (2009) 2728–2733.
[13] T. Sakamoto, H. Kikuchi, T. Miyao, A. Yoshida, S. Naito, Appl. Catal. A Gen. 375 (2010) 156–162.
[14] L. Lin, W. Zhou, R. Gao, S. Yao, X. Zhang, W. Xu, S. Zheng, Z. Jiang, Q. Yu, Nat. Publ. Gr. 544 (2017) 80–83.
[15] J.W. Shabaker, J.A. Dumesic, Ind. Eng. Chem. 43 (2004) 3105–3112.
[16] A.V. Tokarev, A.V. Kirilin, E.V. Murzina, K. Eränen, L.M. Kustov, D.Y. Murzin, J.P. Mikkola, Int. J. Hydrogen Energy 35 (2010) 12642–12649.
[17] T. Sakamoto, T. Miyao, A. Yoshida, S. Naito, Renew. Energy 35 (2010) 6203–6209.
[18] T. Nozawa, A. Yoshida, S. Hikichi, S. Naito, Int. J. Hydrogen Energy 40 (2015) 4129–4140.
[19] T. Nozawa, Y. Mizukoshi, A. Yoshida, S. Naito, Appl. Catal. B Environ. 146 (2014) 221–226.
[20] I.O. Cruz, N.F.P. Ribeiro, D.A.G. Aranda, M.M.V.M. Souza, Catal. Commun. 9 (2008) 2606–2611.
[21] B. Roy, U. Martinez, K. Loganathan, A.K. Datye, C.A. Leclerc, Int. J. Hydrogen Energy 37 (2012) 8143–8153.
[22] B. Roy, C.A. Leclerc, J. Power Sources 299 (2015) 114–124.
[23] A. Wawrzetz, B. Peng, A. Hrabar, A. Jentys, A.A. Lemonidou, J.A. Lercher, J. Catal. 269 (2010) 411–420.
[24] Y. Lei, S. Lee, K. Low, C.L. Marshall, ACS Catal. 6 (2016) 3457–3460.
[25] L.I. Godina, A.V. Tokarev, I.L. Simakova, P. Mäki-Arvela, E. Kortesmäki, J. Gläsel, L. Kronberg, B. Etzold, D.Y. Murzin, Catal. Today 301 (2018) 78–89.
[26] L. Chen, Y. Zhu, H. Zheng, C. Zhang, B. Zhang, Y. Li, J. Chem. Technol. Biotechnol. 87 (2012) 112–122.
[27] L. Chen, Y. Zhu, H. Zheng, C. Zhang, Y. Li, J. Chem. Technol. Biotechnol. 87 (2012) 1089–1097.
[28] I. Coronado, M. Stekrova, L. García Moreno, M. Reinikainen, P. Simell, R. Karinen, J. Lehtonen, Biomass Bioenergy 106 (2017) 29–37.
[29] M. Stekrova, A. Rinta-Paavola, R. Karinen, Catal. Today 304 (2018) 143–152.
[30] A. Iriondo, V.L. Barrio, J.F. Cambra, P.L. Arias, M.B. Güemez, R.M. Navarro, M.C. Sánchez-Sánchez, J.L.G. Fierro, Top. Catal. 49 (2008) 46–58.
[31] A. Chen, H. Guo, Y. Song, P. Chen, H. Lou, Int. J. Hydrogen Energy 42 (2017) 9577–9588.
[32] M.L. Barbelli, F. Pompeo, G.F. Santori, N.N. Nichio, Catal. Today 213 (2013) 58–64.
[33] M.M. Rahman, T.L. Church, A.I. Minett, A.T. Harris, ChemSusChem 6 (2013) 1006–1013.
[34] Y. Guo, M.U. Azmat, X. Liu, Y. Wang, G. Lu, Appl. Energy 92 (2012) 218–223.
[35] N. Luo, X. Fu, F. Cao, T. Xiao, P.P. Edwards, Fuel 87 (2008) 3483–3489.
[36] R.L. Manfro, A.F. Da Costa, N.F.P. Ribeiro, M.M.V.M. Souza, Fuel Process. Technol. 92 (2011) 330–335.
[37] D.A. Boga, R. Oord, A.M. Beale, Y.-M. Chung, P.C.A. Bruijnincx, B.M. Weckhuysen, ChemCatChem 5 (2013) 529–537.
[38] P.V. Tuza, R.L. Manfro, N.F.P. Ribeiro, M.M.V.M. Souza, Renew. Energy 50 (2013) 408–414.
[39] R.L. Manfro, T.P.M.D. Pires, N.F.P. Ribeiro, M.M.V.M. Souza, Catal. Sci. Technol. 3 (2013) 1278–1287.
[40] G. Ertl, H. Knözinger, J. Weitkamp (Eds.), Handbook of Heterogeneous Catalysis, Vol. 2 VCH Verlagsgesellschaft mbH, 1997.
[41] A. Kayode Coker (Ed.), Ludwig's Applied Process Design for Chemical and Petrochemical Plants, Vol. 1 Elsevier Science & Technology, 2007.
[42] R.D. Cortright, R.R. Davda, J.A. Dumesic, Nature 418 (2002) 964–967.
[43] T. van Haasterecht, C.C.I. Ludding, K.P. de Jong, J.H. Bitter, J. Catal. 319 (2014) 27–35.
[44] Y.D. Li, L.Q. Li, H.W. Liao, H.R. Wang, J. Mater. Chem. 9 (1999) 2675–2677.
[45] J.N. Chheda, G.W. Huber, J.A. Dumesic, Angew. Chemie - Int. Ed. 46 (2007) 7164–7183.
[46] M. Mavrikakis, M.A. Barteau, J. Mol. Catal. A Chem. (1998) 135–147.
[47] J.L. Davis, M.A. Barteau, Surf. Sci. 187 (1987) 387–406.
[48] M. Myint, Y. Yan, J.G. Chen, J. Phys. Chem. C 118 (2014) 11340–11349.